



Numerical Investigation of Hydrothermal Characteristics in Backward-Facing Step Channel with Obstacles

Ibrahim K. Alabdaly^{1*}, Saad M. Hatem², Mohammed A. Ahmed², Tareq Hamad Abed³,
Qusay Rasheed Al-Amir⁴

¹ Department of Chemical and Petrochemical Engineering, College of Engineering, University of Anbar, Ramadi 31001, Iraq

² Department of Mechanical Engineering, College of Engineering, University of Anbar, Ramadi 31001, Iraq

³ Renewable Energy Research Centre, University of Anbar, Ramadi 31001, Iraq

⁴ Mechanical Power Engineering Department, College of Engineering and Technologies, Al-Mustaqbal University, Babylon 51001, Iraq

Corresponding Author Email: ibrahim.khadir@uoanbar.edu.iq

Copyright: ©2025 The authors. This article is published by IETA and is licensed under the CC BY 4.0 license (<http://creativecommons.org/licenses/by/4.0/>).

<https://doi.org/10.18280/ijht.430131>

ABSTRACT

Received: 7 September 2024

Revised: 16 January 2025

Accepted: 1 February 2025

Available online: 28 February 2025

Keywords:

numerical study, backward facing step, obstacles, laminar flow, finite volume method

The present numerical work investigates the forced convection fluid flow through a backward-facing step (BFS) in the channel with obstacles. Three different shapes of obstacles which are circular, square and diamond have been considered to enhance the hydrothermal performance. The finite volume procedure has been utilized to resolve the two-dimensional continuity, energy, and momentum equations. Influence of obstacle sizes ($d/H=0.2, 0.3, \text{ and } 0.4$) as well as obstacle locations ($b/H=2, 3, \text{ and } 4$) on the hydrothermal performance factor, pressure losses, and mean Nusselt number have been analyzed for Reynolds number between 200 and 1000. Results indicate that as the Reynolds number rises, the average pressure losses and Nusselt number rise, well the thermal-hydraulic performance factor decreases. The circular obstacle provided the highest heat transfer enhancement (about 49%) at $Re=1000, d/H=0.4, \text{ and } b/H=2$ compared with the baseline case. In addition, the performance factor rises with the reduction in the distance between the obstacles and the step. The best performance factor is around 1.24 which can be obtained utilizing a BFS channel with a circular obstacle at $Re=200, d/H=0.4 \text{ and } b/H=2$, making it the optimal setup for applications requiring efficient thermal management with minimal pressure loss penalties.

1. INTRODUCTION

When studying independent flows in fluid mechanics, backward-facing step flow in a channel is frequently used as a reference design. Heat transfer, including split flow and reconnection, is commonly used in many technological applications. Interesting problems in applied research include fluid dynamics and heat conduction in the return stage. This method addresses a range of practical challenges encountered in industrial settings. Conceptually, challenges of this nature can be used for various industrial gadgets and everyday electronics. These examples pertain to various areas such as industrial operations, the flow of air behind vehicles, the flow of air into a tunnel for engines, heat exchange in condensers and combustion chambers, and the cooling of electronic chips and devices. Therefore, numerous experimental, numerical, and analytical investigations focused on these phenomena may be found in various sources [1].

Iwai et al. [2] studied the impact of the channel dimensions on discharges encountered at low Re numbers over a BFS. The discoveries indicated that when the aspect ratio grew, the heat transfer through the lower surface exhibited a higher value and shifted upstream in location. Increasing the aspect ratio also

raised the coefficient of friction losses. In all cases, the highest Nu was seen along both side surfaces, rather than on the lower wall centerline. The optimum Nu improved as the Re raised, and its place along the streamwise trend carried downstream. Abu-Nada [3] used different volume rates of nanoparticles to perform a computer examination of heat transfer improvement through a BFS. Results found that excluding the primary and secondary vortices areas, all areas of the walls saw a rise in the Nu as the Re increased. The effects of blowing and suction on the flow and thermal systems through a BFS were investigated by Abu-Nada et al. [4]. It was discovered that the regional Nu at the top surface is the reverse of that on the lower wall, where it decreases by blowing and increases by suction. The reattachment point on the bottom wall has the greatest local Nusselt number. In the upper wall, high rates of suction bleed and high Re numbers indicate maximum average Nusselt number values. Khanafer et al. [5] analyzed the heat transfer under pulsing configurations using a (BFS) in 2D laminar mixed convection flow. The findings demonstrated the significant effect of dimensionless oscillation frequency, Richardson number, and Re number on the features of thermal and fluid flow. Kondoh et al. [6] examined the aspect of BFS concerning laminar heat transfer. Along with the local and

peak Nusselt numbers, they also provided the thermal front and their locations. They reported that the reattachment location does not always correspond with the highest Nu value. Nie and Armaly [7] examined the influence on laminar fluid flow and the thermal features of the step size of the BFS channel. They discovered that the average heat improvement and the prime vortex area increased in conjunction with the step height. Furthermore, in a prime re-circulation area, a highest friction coefficient occurred when the height of the step was raised. Abedalh et al. [8] carried out an empirical analysis of the thermal and flow fields over a BFS channel under a laminar regime. Their results showed that the friction factor reduced when Re increased. Furthermore, the mean Nu increased in association with Re.

Several researchers have focused on the effects of a step channel facing backwards and a corrugated surface or rib (sometimes called a turbulator) on thermal and fluid discharge properties. A cylinder of different diameters put after the step disrupted the flow, lowering the crossing angle of the temperature gradient and velocity vector and increasing the rate of heat transfer, as demonstrated numerically and analytically by Kumar and Dhiman [9]. Outcomes displayed that the peak and mean Nu grew gradually with Re number and that the most elevated Nu was improved by up to 155% compared with the baseline choice (without a cylinder). Kumar and Vengadesan [10] studied the influence of the fin on the upper wall of a BFS with uniform lower surface temperature, which was quantitatively examined for 2D laminar heat transfer and fluid flow features by numerical simulation. They observed that increasing velocity amplitude improves the average Nusselt number, whereas increasing oscillation amplitude did not affect it at a constant velocity amplitude. Ahmed et al. [11] analysed the low Re regime forced convection affects the discharge of fluids and the movement of heat through a micro-scale backwards-facing step MBFS channel that has various kinds of turbulators. Their outcomes showed that adding a vortex generator to MBFS raises both the Nu and the pressure losses at the same time. The performance evaluation criterion (PEC) goes up as the Re number goes up until the number 180. After that, a sharp drop has been seen. Li et al. [12] numerically studied the additional influence of various porous baffles in a backwards-facing step to improve flow analysis and thermal system. In their investigation, the effect of various parameters including size of baffles, baffle location, Re number, and Darcy number on the thermal and flow pattern. Outcomes showed that the improvement of heat transfer is up to 35% at a Re number of 500. Also, the heat transfer rates improved by 32% at a porous baffle height of 1.5.

Tsay et al. [13] Investigated the effect of a vertically placed baffle on the convective characteristics of (BFS) flow. When comparing the outcomes of cases without and with a baffle, it was found that the mean Nu increased by nearly 190% throughout the heating phase and 150% in the heating portion of the lower surface. Eleiwi et al. [14] demonstrated the influence of three non-rotating cylinders in the BFS channel on the laminar flow field and heat transfer augmentation. BFS flow is investigated for the influences of heat fluxes, Re number, and the space between two following cylinders on the thermal features. Using cylinders reduced the distance of flow reattachment. It was noted that as the heat fluxes rise by 67%, the Re number changes from 50 to 250, leading to a heat transfer augmentation of 6% to 13%. Cheng and Tsay [15] and Ma et al. [16] examined the influences on the features of the

thermal system and flow field of various baffle designs in two-dimensional laminar BFS channels. They exposed a notable growth in the heat transfer improvement followed by an approximate rise in the pressure drop when the Reynolds number increased. Boruah et al. [17] examined the thermohydraulic features and the entropy production of a mixed convective flow via a (BFS) channel with three various baffle shapes such as; (triangular, square and elliptical) baffles at the upper wall. They observed that the square baffle has the highest mean Nu value, whereas the elliptical baffle has the lowest entropy generation. Selimefendigil and Öztop [18], and Anguraj and Palraj [19] studied the influence of rotating single-cylinder on the flow and thermal features across (BFS). It is discovered that flow in the wake region after the cylinder will depend on its rotation orientation. Furthermore, for low Re numbers, in particular, the distribution of the local Nu is changed by the rotation. It has previously been investigated to use ribs upstream of the step to regulate the separation region in the BFS channel by Barsukov et al. [20]. Findings showed that a single rib significantly changes turbulent fluctuations and average streamwise velocity profiles while also shortening the reattachment length. Abdollahpour et al. [21] examined how the cylinder affected the discharge across a stage channel that faced backwards and discovered that using a cylinder increased the skin friction coefficient in the reverse flow zone.

In this investigation, a laminar forced convection outpour via a BFS channel with obstacles is numerically investigated for Reynolds number range 200-1000. Effects of Reynolds number, the sizes and positions of obstacles on the water outpour and thermal factors are shown and examined.

The outlines of the present study explained in the upcoming sections is as follows: The description of the current investigation is included in the second part. The third part contains the border conditions and governing equations. The numerical explanation of the current problem is presented in the fourth section. The grid independence test and the validity of the calculated results are demonstrated in section 5. The sixth part presents the results and discussion, while the seventh section presents the conclusions.

2. PROBLEM DEPICTION AND ASSUMPTIONS

A physical domain of the current investigation is depicted in Figure 1.

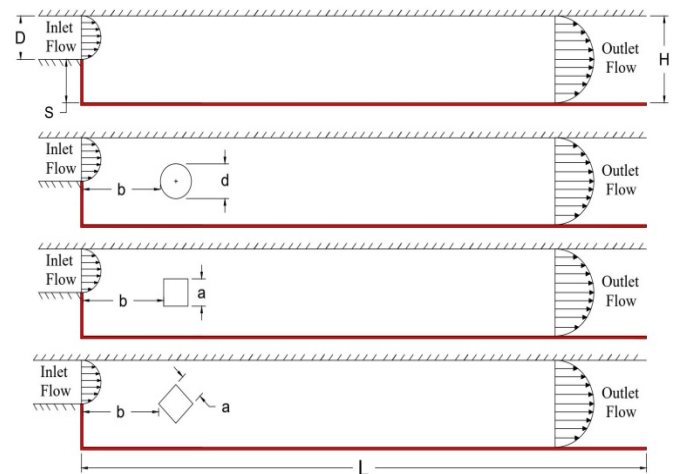


Figure 1. Geometry of the current investigation

It contains of two surfaces which are the lower and upper surfaces with intake height D , outlet channel height ($H=10$ mm), step height (S), and channel length (L). Three different obstacle shapes: circular with a diameter of (d), square and diamond with a side length of (a) are located inside the channel at a distance (b) from the intake. In this analysis, all the obstacle shapes have the same surface area. The geometry parameters are studied in a non-dimensional form depending upon the channel height (H) as follows: ($L/H=20$), ($S/H=0.5$), ($d/H=0.2, 0.3$ and 0.4) as well as ($b/H=1, 2$, and 3). It is considered that the water flow in the channel is two-dimensional, laminar, incompressible, steady, and subject to a boundary condition of no-slip velocity at all surfaces. The flow at the BFS channel entrance is presumed to be fully developed at a constant temperature of ($T=300$ K). The step and bottom surfaces of the BFS channel are subjected to uniform heat flux and the other surfaces are adiabatic.

3. GOVERNING EQUATIONS AND BOUNDARY CONDITIONS

The two-dimensional governing equations for momentum, continuity, and energy in the cartesian coordinates form are summarized for incompressible, fully developed, single-phase, steady-state, and laminar flow. Therefore, the coordinate system used for the governing equations can be expressed as [22, 23]:

Continuity equation:

$$\frac{\partial}{\partial x}(\rho u) + \frac{\partial}{\partial y}(\rho v) = 0 \quad (1)$$

X-momentum equation:

$$\frac{\partial}{\partial x}(\rho uu) + \frac{\partial}{\partial y}(\rho vu) = \mu \left[\frac{\partial^2 u}{\partial x^2} + \frac{\partial^2 u}{\partial y^2} \right] - \frac{\partial p}{\partial x} \quad (2)$$

Y-momentum equation:

$$\frac{\partial}{\partial x}(\rho uv) + \frac{\partial}{\partial y}(\rho vv) = \mu \left[\frac{\partial^2 v}{\partial x^2} + \frac{\partial^2 v}{\partial y^2} \right] - \frac{\partial p}{\partial y} \quad (3)$$

Energy equation:

$$\frac{\partial}{\partial x}(\rho uT) + \frac{\partial}{\partial y}(\rho vT) = \frac{\mu}{Pr} \left[\frac{\partial^2 T}{\partial x^2} + \frac{\partial^2 T}{\partial y^2} \right] \quad (4)$$

Table 1. Thermophysical properties of water [3]

ρ (kg/m ³)	k (W/m K)	C_p (J/kg K)	α (m ² /s)
997.1	0.613	4179	1.47×10^{-7}

The primary boundary condition is achieved for backward-facing step channels to streamline the computational explanation. The upper surface is applied to the adiabatic and no-slip conditions ($Q=0$). Meanwhile, the unchanging heat flux ($Q=4000$ W/m²) is set up on a lower and step walls. The Reynolds number ($Re=200-1000$) determines the entrance velocity, and the water temperature at the inlet is 300 K. The condition of the end channel is assumed to be employed at the value of ($P_{out}=P_{gage}$) to avoid reversed flow. Pure water is used

as a working (see Table 1 for thermophysical properties of working liquid) [3].

4. NUMERICAL SOLUTION

The boundary conditions, governing equations, and assumptions were utilized to solve the problem of THE investigated computational domain. Based on the ANSYS-FLUENT V.20, the governing equations and chaperoning boundary conditions were resolved by utilising the finite volume approach (FVM) [24]. The upwind approach is chosen to discretize the governing equations' convection terms. In contrast, the flow field of the current study is solved by employing the SIMPLE algorithm [25]. The momentum and energy equations' term of diffusion is represented by the second upwind difference [26]. All cells follow the discrete conservation equations of momentum, energy, and continuity at convergence. When utilizing residuals to monitor convergence, it becomes evident that the solution remains unchanged after additional iterations. The current work's residual continuity, energy, and momentum equation is about 10^{-5} .

The mean Nusselt number, pressure losses, and the PEC will be calculated once the governing equations have been solved using the thermal and flow field data. Hence, the average Nusselt number at the step and lower surfaces can be illustrated as [11, 27]:

$$Nu_{ave.} = \frac{h D}{K} \quad (5)$$

The pressure drop can be expressed as:

$$\Delta P = P_{in} - P_{out} \quad (6)$$

The PEC factor can be calculated as [28, 29]:

$$PEC = \left(\frac{Nu_{ave,withobstacle}}{Nu_{ave,withoutobstacle}} \right) / \left(\frac{f_{withobstacle}}{f_{withoutobstacle}} \right)^{1/3} \quad (7)$$

If the friction factor, denoted by f , can be written as [30-32]:

$$f = \Delta P \frac{D}{L} \frac{2}{\rho u_{in}^2} \quad (8)$$

5. GRID-INDEPENDENCE STUDY AND MODEL VALIDATION

The computational grids of the backward-facing step provided with and without different obstacle shapes are constructed by utilizing ANSYS software's DesignModeler. To confirm the precision of the present investigation, the mesh must be developed and controlled in the two-dimensional model before assessing the grid's dependencies and quality for a prior run. Thus, enough cells are needed for valid results (see Figure 2). The mesh generation around the obstacles was carefully controlled in order to reduce the numerical errors and ensure smooth flow variation. The grid-independent test is studied to discover a sufficient grid system for the backwards-facing step channel with a circular obstacle at $Re=1000$, $d/H=0.4$, and $b/H=2$. Five various grid sizes are tried, from

8,960 to approximately 99,000. The mesh generated for the current investigation includes around 24,800 nodes, where the comparative deviation between the third and fourth grid sizes is 0.6% for the mean Nu and 0.8% for the pressure drop. The best (third) grid ensures no change in the mean Nu and pressure losses. Therefore, the mesh of 24,800 nodes is utilized in the current research. Figure 3 displays the Nu and pressure loss values with the mesh sizes.

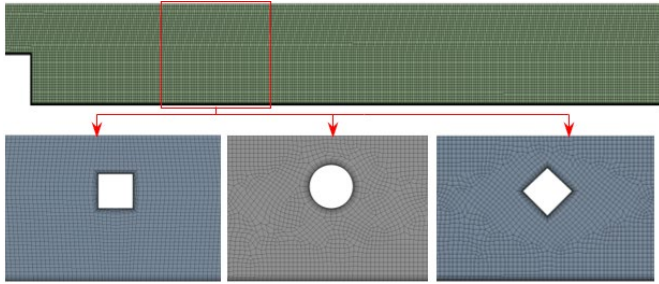


Figure 2. Grid generation of the current analysis at $d/H=0.4$, and $b/H=2$

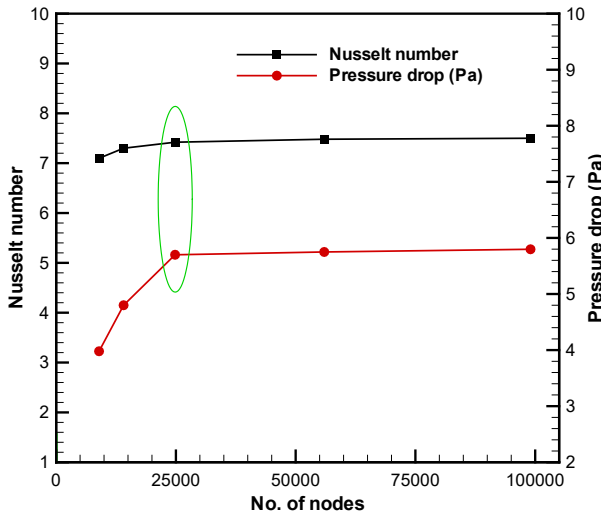


Figure 3. Grid independence check of the current investigation at $d/H=0.4$, $Re=1000$, and $b/H=2$

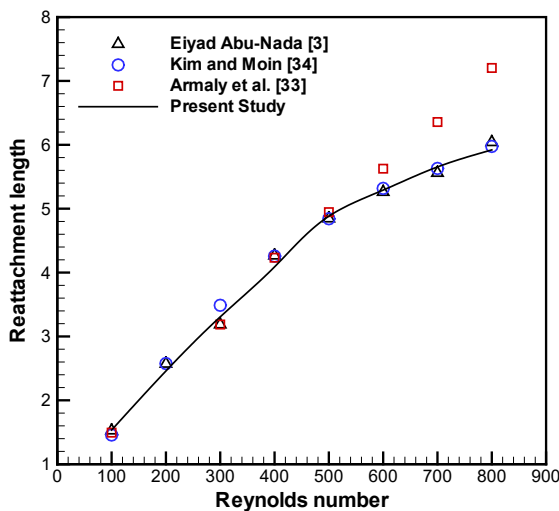


Figure 4. Compare the present investigation findings with earlier experimental and numerical outcomes

A length of a two-dimensional horizontal BFS reattachment

was measured and compared with various numerical values produced by Abu Nada [3], the practical research of Armaly et al. [33], and the numerical outcomes of Kim and Moin [34] to verify the current study's findings at aspect ratio of ($AR=2.0$) and $Pr=0.7$. Figure 4 indicates that the data demonstrate a high degree of agreement.

6. RESULTS AND DISCUSSION

The following sections of the study present and discuss the influences on the thermal and fluid flow fields of the Reynolds number ($Re=200-1000$), the shapes of the obstacles (circular, square, and diamond), the obstacle sizes ($d/H=0.2, 0.3$, and 0.4), and the obstacle locations ($b/H=1, 2$, and 3).

6.1 Effects obstacle shapes

Figures 5 and 6 show the contours of streamline and isotherm in a backwards-facing step channel using three shapes of obstacles (circular, square, and diamond). These results are compared with the channel without any obstacle at $Re=1000$, $b/H=3$, and $d/H=0.3$.

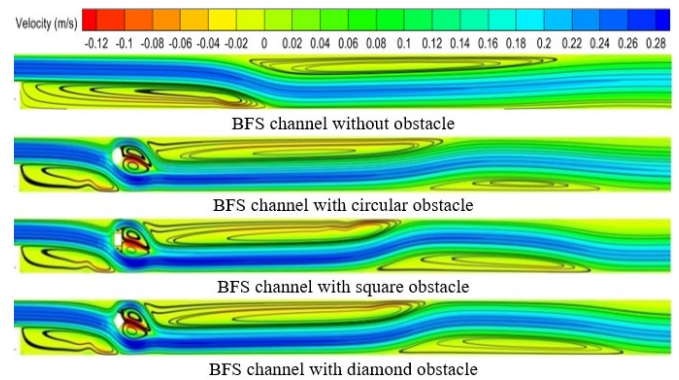


Figure 5. Velocity streamline for different obstacles shapes at $Re=1000$, $b/H=3$, and $d/H=0.3$

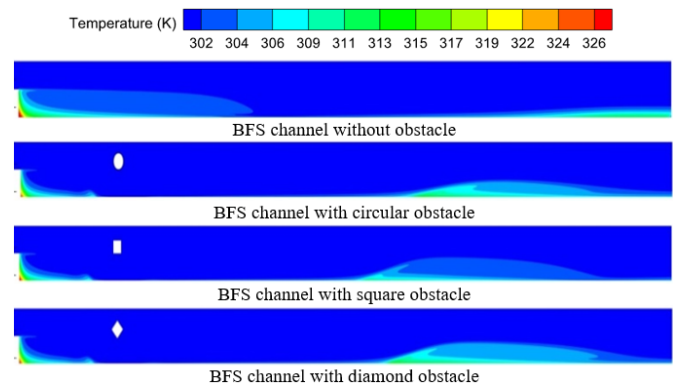


Figure 6. Temperature contours for different obstacles shapes at $Re=1000$, $b/H=3$, and $d/H=0.3$

As the fluid flowing over the step channel without obstacles, it detaches from the inlet surface to create a primary vortex (recirculation zone) immediately downstream of the step near the lower- heated wall. This is clear because there are closed streamlines near the step, meaning a primary vortex exists. The reattachment of the flow occurs at some location further downstream on the lower surface, where the streamlines are once again parallel and fully developed. Otherwise, the

secondary vortex is developed at the adiabatic top wall of the BFS channel because of the impact of the step on the top surface. The addition of various shapes of obstacles inside the channel has proved that these obstacles created wake zones behind them. These zones are characterized by a recirculation zone or vortex, indicated by the closed streamlines behind the obstacle. The obstacle gives rise to some kind of interplay that brings a level of complexity to the flow, which produces extra vortices near the bottom wall that could increase the diffusivity of the fluids, affecting mixing and improving heat transfer in the channel. Further, using various obstacles of varied forms decreased the sizes and intensity of the primary recirculation in the channel.

While considering the temperature contours (Figure 6), the high thermal boundary layer (TBL) thickness downstream of the step region is because of primary recirculation. It can be indicated that the adding obstacles inside the BFS channel led to a decrease in the thickness of the TBL downstream of the step. Further, a vortex within the BFS channel would enhance fluid mixing, predominantly behind obstacles. These kinds of enhancements in mixing disturb the thermal boundary layers and hence result in local heat transfer rates that are generally higher. Besides, a square obstacle with sharp corners leads to a greater decrease in the TBL thickness downstream of the obstacle compared with other obstacles. This outcome is comparable to the previous outcomes notified by Boruah et al. [17].

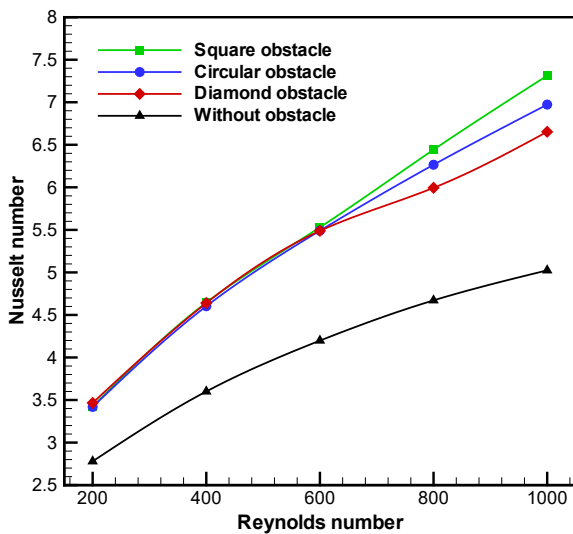


Figure 7. Influence of different obstacle shapes on the mean Nusselt number at $b/H=3$, and $d/H=0.3$

Figure 7 shows the relation between the Re and the mean Nu for various obstacle shapes at $b/H=3$, and $d/H=0.3$, compared with a channel without obstacles. For all cases, the Nusselt number rises with the rising Re due to the height in the gradient of temperature at the step and lower surfaces. Furthermore, the baseline case (without any obstacle) displays the lowest Nu for all values of Re numbers. Therefore, the presence of obstacles enhances the heat transfer process by disturbing the flow and fluid mixing. In addition, the square obstacle produces the highest Nu for $Re > 600$. This means that the square shape creates the most effective disturbance in the flow, due to the sharp edges causing strong vortices and turbulent mixing. The enhancement percentages in the Nu are approximately (46, 39, and 32) % for square, circular, and diamond, respectively at $Re=1000$, $b/H=3$, and $d/H=0.3$,

compared with the baseline case. This trend is identical to the previous outcomes noted by Eleiwi et al. [14].

Figure 8 illustrates the variation of the pressure losses with Re for various obstacle shapes at $b/H=3$, and $d/H=0.3$, compared with the baseline case. It is shown that the pressure drop enlargements as the Reynolds number grows for all cases because the frictional forces and flow disturbances within the channel growth with the Reynolds number. Furthermore, it is found that the base case displays the lowest pressure drop compared with other cases which produce significantly higher pressure drops. It can be found that the pressure drop of the both square and diamond obstacles provided the highest values among all the cases due to the sharp edges that cause strong flow separation and turbulence, leading to higher energy losses. Moreover, the circular obstacle results in a lower pressure drop compared to the square and diamond obstacles, but higher than the no-obstacle case. The rounded edges of the circular shape cause less severe flow separation, leading to less flow resistance and, therefore, a lower pressure drop.

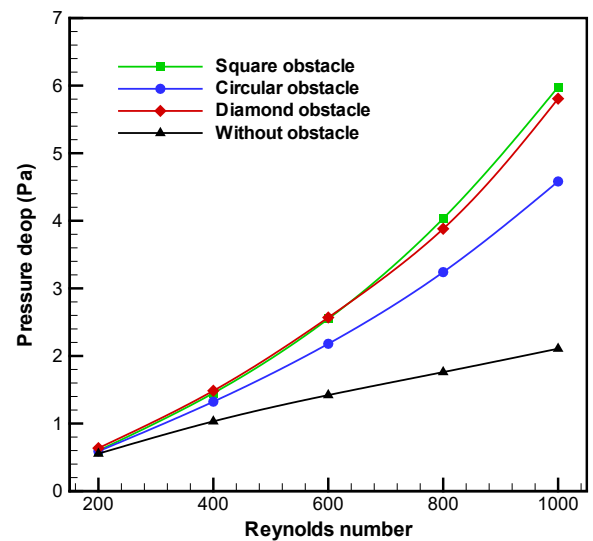


Figure 8. Influence of different obstacles shapes on the pressure drop at $b/H=3$, and $d/H=0.3$

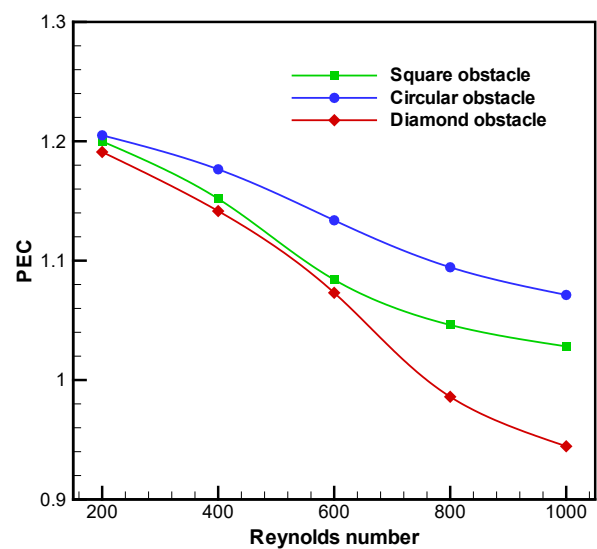


Figure 9. Effect of different obstacles shapes on the thermal-hydraulic performance factor at $b/H=3$, and $d/H=0.3$

Figure 9 displays the relation between the PEC and the

Reynolds number for various obstacle forms at $b/H=3$, and $d/H=0.3$, compared with the baseline case. It is found that the PEC decreases as Re numbers increase for all cases. This indicates that as the flow becomes more tumultuous, the pressure drop penalty rises faster than the heat transfer enhancement for all obstacle shapes. Further, the maximum PEC obtained at the circular obstacle is about 1.2 at $Re=200$, followed by the square shape and diamond-shaped obstacle has the lowest PEC, particularly at higher Re. Results concluded that the circular obstacle is the most efficient design according to the thermal-hydraulic performance factor in terms of heat transfer improvement and pressure losses across the studied Reynolds numbers.

6.2 Effects of obstacle sizes

Figures 10 and 11 illustrate the velocity and temperature contours for different obstacle sizes ($d/H=0.2, 0.3$, and 0.4) within the BFS channel at $Re=800$, and $b/H=3$.

For the velocity streamline (Figure 10), it is observed that when the obstacle size increases, the recirculation behind the circular obstacle increases which leads to improved fluid mixing and heat transfer enhancement as well as rises in the pressure losses. In addition, it can be noticed that with the increase of obstacle size, there exists a reduction in the cross-sectional area of the fluid stream resulting in a rise in the fluid velocity and heat transfer enhancement at the bottom of the obstacle. Moreover, it is observed that as the d/H increases, the size of the secondary recirculation which is created near the upper wall increases. This analysis indicates that the obstacle size significantly influences the flow behaviour downstream of the BFS channel.

For the temperature contours (Figure 11), It is noted that the obstacle sizes have a significant influence on the temperature contours. Furthermore, results indicate that the thickness of the TBL decreases as the obstacle sizes increase at the bottom obstacle. This development is identical to the previous influences noted by Tsay et al. [13].

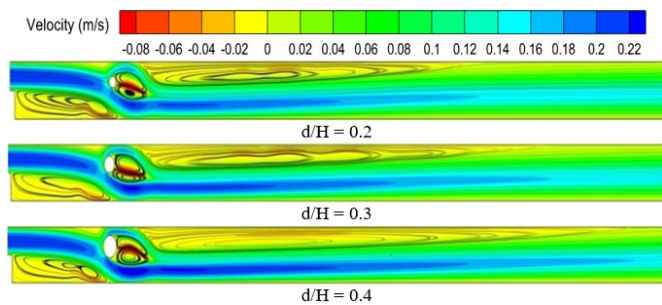


Figure 10. Velocity contours for different obstacle sizes at $Re=800$, and $b/H=3$

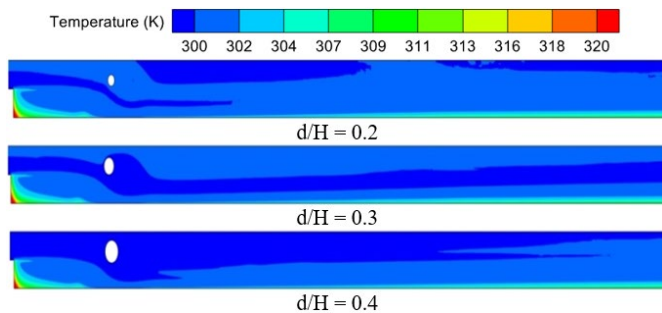


Figure 11. Isotherms contours for different obstacle sizes at $Re=800$, and $b/H=3$

The effect of the circular obstacle sizes ($d/H=0.2, 0.3$ and 0.4) on the Nu for the Reynolds number of ($Re=200-1000$) at $b/H=3$ is presented in Figure 12. As Reynolds number increases, the mean Nusselt number increases for all cases due to the increase in the temperature gradient. In addition, the average Nu increases as the obstacle sizes increase because the large sizes of the obstacles provide improved fluid mixing and heat transfer enhancement. The maximum enhancement percentage of the mean Nusselt number was (about 45%) obtained at $Re=1000$, the circular obstacle sizes of ($d/H=0.4$), and the obstacle location of ($b/H=3$).

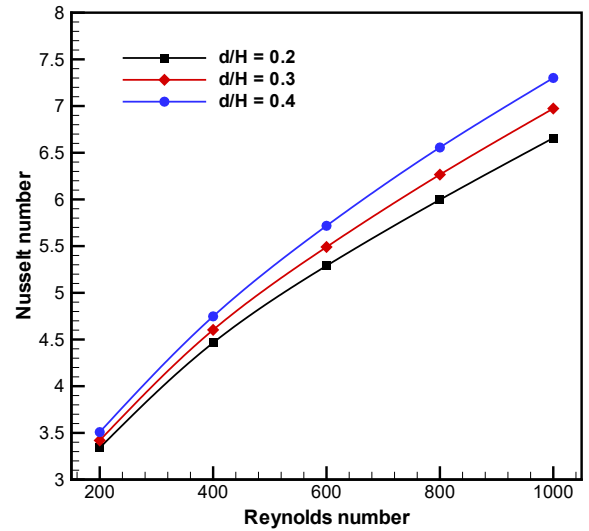


Figure 12. Influence of different obstacle sizes on the average Nusselt number at $b/H=3$

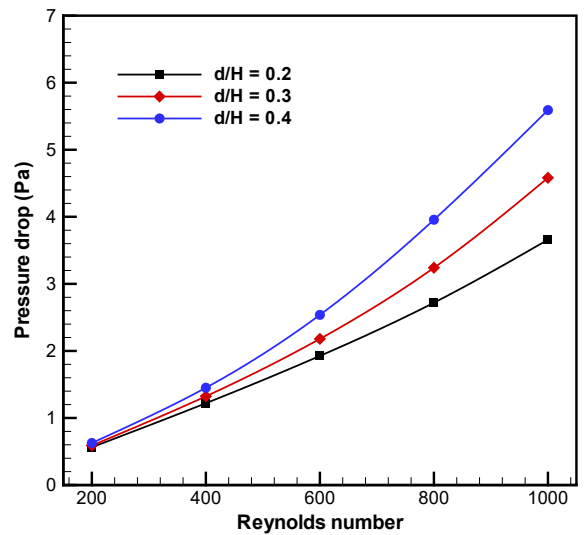


Figure 13. Influence of different obstacle sizes on the pressure drop at $b/H=3$

Figure 13 represents the relation of the pressure losses and Re for various obstacle sizes at $b/H=3$. For all obstacle sizes, it is found that the pressure losses increase with Re. Further, large circular obstacle sizes produced high-pressure losses. This is due to that as the obstacle sizes increase, the reverse flow behind the obstacle increases which leads to increased obstruction of fluid flow within the BFS channel.

Figure 14 explains the relation between the PEC and Re for different obstacle sizes at $b/H=3$. The PEC, which accounts for both heat transfer and pressure losses, decreases with

increasing Re number for all obstacle sizes. Moreover, bigger obstacles have a higher PEC, particularly at low Re due to a more efficient heat transfer relative to the pressure drop. Further, the small obstacle ($b/H=2$) size has the maximum PEC at high Re due to the heat transfer enhancement outweighing the increasing in the pressure losses.

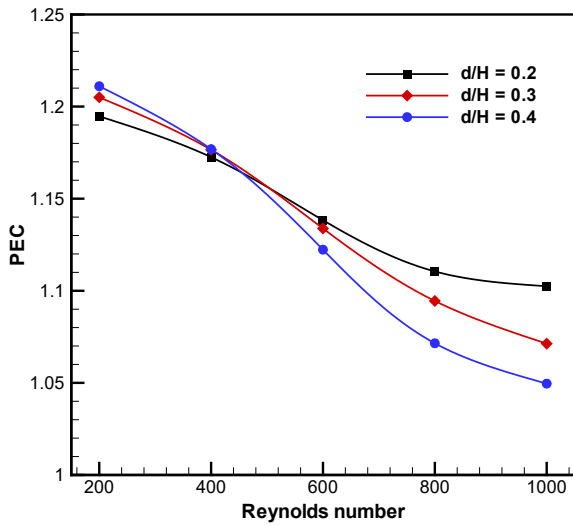


Figure 14. Influence of different obstacle sizes on the thermal-hydraulic performance factor at $b/H=3$

It can be concluded that the use of the biggest obstacle size of ($b/H=4$) provided the highest value of PEC (approximately 1.21) at $Re=1000$ and $b/H=3$.

6.3 Effects of obstacle locations

Figures 15 and 16 present the effect of the circular obstacle locations ($b/H=2, 3, \text{ and } 4$) on the velocity and temperature contours in BFS channels at $Re=800$, and $d/H=0.4$.

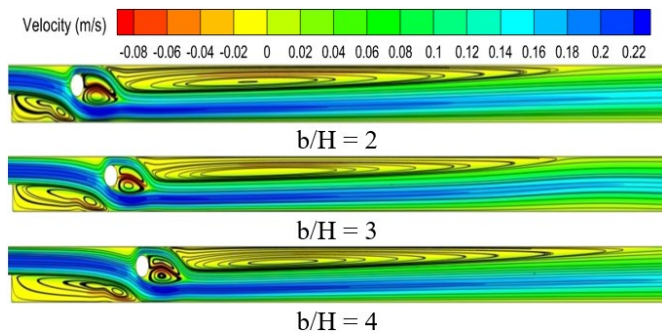


Figure 15. Velocity streamline for different obstacle locations at $Re=800$, and $d/H=0.4$

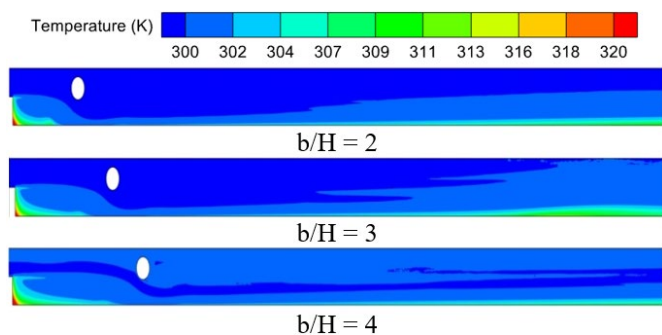


Figure 16. Isotherms contours for different obstacle locations at $Re=800$, and $d/H=0.4$

For the streamwise velocity (Figure 15), it is observed that the different circular obstacle locations have an effective influence on the velocity distribution inside the BFS channels. Further, the size and intensity of the primary vortex increase as the distance between the obstacle and the step. Moreover, as the b/H increases, the location of the secondary vortex (at the upper wall) moves forward downstream of the obstacle.

For the temperature contours (Figure 16), it is remarked that the thermal boundary thickness downstream of the step rises as the distance between the obstacle and the step increases. This is because as the b/H increases, the size of the primary vortex grows, which leads to a thickening of the TBL.

Figure 17 presents the variation of the Nu with the Re for different distances between the obstacle and the step ($b/H=2, 3, \text{ and } 4$) at $d/H=0.4$. As expected, for all values of b/H , the Nusselt number increases with increasing Reynolds number. When the distance between the circular obstacle and the step is small ($b/H=2$), the Nu is higher in terms of the Re. Further, The Nusselt number decreases with increasing distance for $b/H=3$ and 4. This is because the thermal boundary layer thickness is low when the obstacle level is at $b/H=2$ and increases with increasing the b/H (see Figure 16). The highest improvement percentage of the mean Nusselt number was (about 49%) obtained at $Re=1000$, the circular obstacle sizes of ($d/H=0.4$), and the obstacle location of ($b/H=2$). This analysis highlights the significant influence of obstacle placement on heat transfer in the BFS configuration.

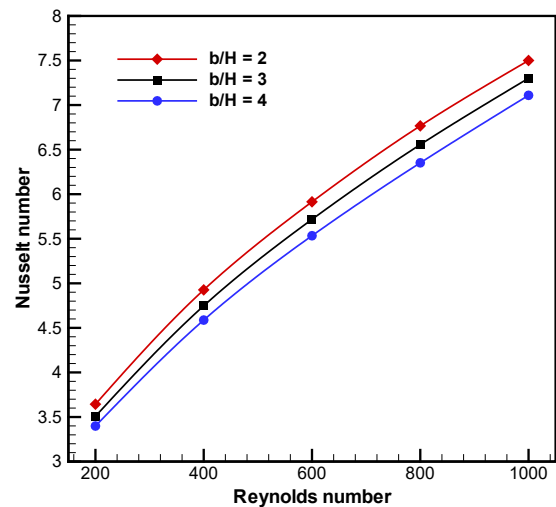


Figure 17. Influence of different obstacle locations on the mean Nusselt number at $d/H=0.4$

Figure 18 illustrates the effect of the circular obstacle locations on the pressure drop for $Re=200-1000$ at $d/H=0.4$. As Re increases, it is found that the pressure losses increase for all cases. When the obstacle is closer to the step ($b/H=2$), the pressure drop is higher across all Reynolds numbers compared to larger distances ($b/H=3$ and 4). This is because the proximity of the obstacle to the step results in a more significant obstruction to the flow, causing higher pressure losses.

Figure 19 displays the influence of the PEC as a function of the Reynolds number for different obstacle locations at $d/H=0.4$. It is shown that the PEC reductions with rising Reynolds number for all distances. Results indicated that all values of PEC are more than unity. Moreover, a smaller distance between the circular obstacle and the step ($b/H=2$) produced a maximum PEC (about 1.24 at $Re=200$) compared

with other cases. This is due to the increased heat transfer efficiency at smaller distances, despite the accompanying higher pressure drop. It can be deduced that the best selection for the location of the obstacle is $b/H=2$ because it provides a better trade-off between the heat transfer improvement and pressure losses.

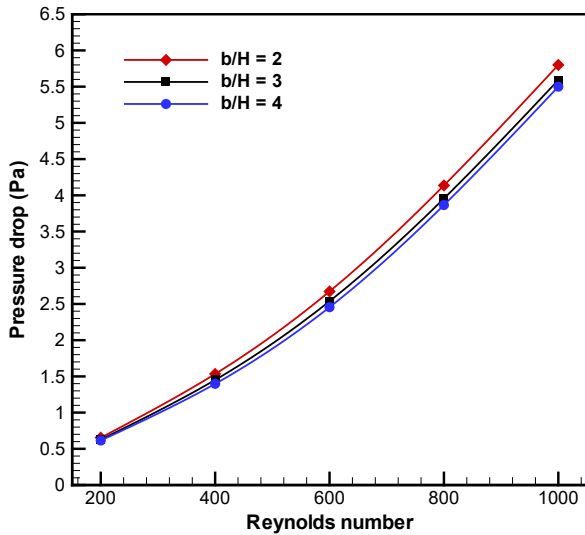


Figure 18. Effect of different obstacle locations on the pressure losses at $d/H=0.4$

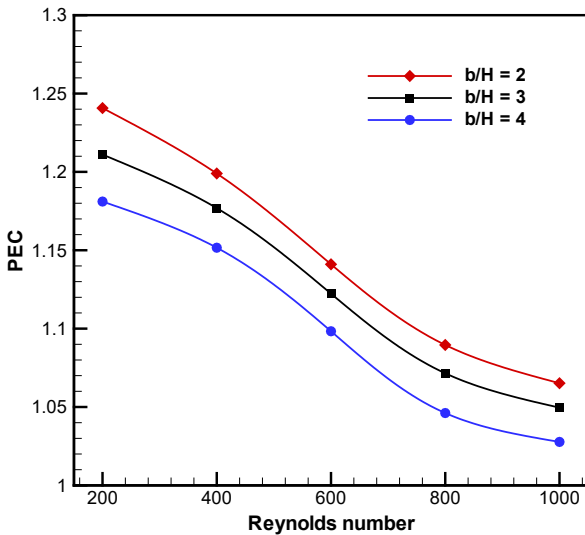


Figure 19. Effect of different obstacle locations on the thermal-hydraulic performance factor at $d/H=0.4$

7. CONCLUSIONS

In the current paper, the effect of obstacles with different shapes on the hydrothermal characteristics in a backward-facing step channel is numerically investigated for Reynolds number range of 200-1000. Three various shapes of obstacles were considered via the BFS channel: circular, square and diamond. The governing equations for continuity, momentum, and energy in two-dimensional systems are solved using the finite volume method. Based on the previous outcomes, the following deductions can be outlined:

- The mean Nusselt number and pressure losses increase with the Reynolds number.
- The average Nusselt number, pressure losses, and

performance factor increase with obstacle size.

- The average Nusselt number, pressure drop and performance factor increase as the distance between the step and the obstacle decreases for a given Reynolds number.

- The circular obstacle can provide the highest performance factor followed by square and diamond shapes.

- The most elevated enhancement ratio of the average Nusselt number was (about 49%) obtained at $Re=1000$, the circular obstacle sizes of ($d/H=0.4$), and the obstacle location of ($b/H=2$).

- The highest performance factor is about 1.24 which can be obtained using BFS channel with circular obstacle at $d/H=0.4$, $b/H=2$ and $Re=200$.

In order to provide the finest hydrothermal performance and a more compact design, the backward-facing step channel with circular obstruction is quantitatively instructed as the ideal design for heat exchangers. The insights gained from this study can be applied to designing efficient cooling systems, compact heat exchangers, and thermal management systems for industrial and electronic applications.

REFERENCES

- [1] Issakhov, A., Zhandaulet, Y., Abylkassyomova, A., Sakypbekova, M., Issakhov, A. (2021). Mixed convection in a channel with buoyancy force over backward and forward facing steps: The effects of inclination and geometry. *Case Studies in Thermal Engineering*, 26: 101152. <https://doi.org/10.1016/j.csite.2021.101152>
- [2] Iwai, H., Nakabe, K., Suzuki, K. (2000). Flow and heat transfer characteristics of backward-facing step laminar flow in a rectangular duct. *International Journal of Heat and Mass Transfer*, 43(3): 457-471. [https://doi.org/10.1016/S0017-9310\(99\)00140-4](https://doi.org/10.1016/S0017-9310(99)00140-4)
- [3] Abu-Nada, E. (2008). Application of nanofluids for heat transfer enhancement of separated flows encountered in a backward facing step. *International Journal of Heat and Fluid Flow*, 29(1): 242-249. <https://doi.org/10.1016/j.ijheatfluidflow.2007.07.001>
- [4] Abu-Nada, E., Al-Sarkhi, A., Akash, B., Al-Hinti, I. (2007). Heat transfer and fluid flow characteristics of separated flows encountered in a backward-facing step under the effect of suction and blowing. *ASME Journal of Heat and Mass Transfer*, 129(11): 1517-1528. <https://doi.org/10.1115/1.2759973>
- [5] Khanafer, K., Al-Azmi, B., Al-Shammari, A., Pop, I. (2008). Mixed convection analysis of laminar pulsating flow and heat transfer over a backward-facing step. *International Journal of Heat and Mass Transfer*, 51(25-26): 5785-5793. <https://doi.org/10.1016/j.ijheatmasstransfer.2008.04.060>
- [6] Kondoh, T., Nagano, Y., Tsuji, T. (1993). Computational study of laminar heat transfer downstream of a backward-facing step. *International Journal of Heat and Mass Transfer*, 36(3): 577-591. [https://doi.org/10.1016/0017-9310\(93\)80033-Q](https://doi.org/10.1016/0017-9310(93)80033-Q)
- [7] Nie, J.H., Armaly, B.F. (2002). Three-dimensional convective flow adjacent to backward-facing step-effects of step height. *International Journal of Heat and Mass Transfer*, 45(12): 2431-2438. [https://doi.org/10.1016/S0017-9310\(01\)00345-3](https://doi.org/10.1016/S0017-9310(01)00345-3)
- [8] Abedalh, A.S., Shaalan, Z.A., Yassien, H.N.S. (2021).

- Mixed convective of hybrid nanofluids flow in a backward-facing step. *Case Studies in Thermal Engineering*, 25: 100868. <https://doi.org/10.1016/j.csite.2021.100868>
- [9] Kumar, A., Dhiman, A.K. (2012). Effect of a circular cylinder on separated forced convection at a backward-facing step. *International Journal of Thermal Sciences*, 52: 176-185. <https://doi.org/10.1016/j.ijthermalsci.2011.09.014>
- [10] Kumar, S., Vengadesan, S. (2019). The effect of fin oscillation in heat transfer enhancement in separated flow over a backward facing step. *International Journal of Heat and Mass Transfer*, 128: 954-963. <https://doi.org/10.1016/j.ijheatmasstransfer.2018.09.001>
- [11] Ahmed, H.E., Kherbeet, A.S., Ahmed, M.I., Salman, B.H. (2018). Heat transfer enhancement of micro-scale backward-facing step channel by using turbulators. *International Journal of Heat and Mass Transfer*, 126: 963-973. <https://doi.org/10.1016/j.ijheatmasstransfer.2018.05.082>
- [12] Li, C., Cui, G., Zhai, J., Chen, S., Hu, Z. (2020). Enhanced heat transfer and flow analysis in a backward-facing step using a porous baffle. *Journal of Thermal Analysis and Calorimetry*, 141: 1919-1932. <https://doi.org/10.1007/s10973-020-09437-w>
- [13] Tsay, Y.L., Chang, T.S., Cheng, J.C. (2005). Heat transfer enhancement of backward-facing step flow in a channel by using baffle installation on the channel wall. *Acta Mechanica*, 174: 63-76. <https://doi.org/10.1007/s00707-004-0147-5>
- [14] Eleiwi, M.A., Tahseen, T.A., Hameed, A.F. (2020). Numerical study of fluid flow and heat transfer in a backward facing step with three adiabatic circular cylinder. *Journal of Advanced Research in Fluid Mechanics and Thermal Sciences*, 72(1): 80-93. <https://doi.org/10.37934/arfmts.72.1.8093>
- [15] Cheng, J.C., Tsay, Y.L. (2006). Effects of solid and slotted baffles on the convection characteristics of backward-facing step flow in a channel. *Heat and Mass Transfer*, 42: 843-852. <https://doi.org/10.1007/s00231-005-0051-0>
- [16] Ma, Y., Mohebbi, R., Rashidi, M.M., Yang, Z., Fang, Y. (2020). Baffle and geometry effects on nanofluid forced convection over forward-and backward-facing steps channel by means of lattice Boltzmann method. *Physica A: Statistical Mechanics and its Applications*, 554: 124696. <https://doi.org/10.1016/j.physa.2020.124696>
- [17] Boruah, M.P., Randive, P.R., Pati, S. (2018). Hydrothermal performance and entropy generation analysis for mixed convective flows over a backward facing step channel with baffle. *International Journal of Heat and Mass Transfer*, 125: 525-542. <https://doi.org/10.1016/j.ijheatmasstransfer.2018.04.094>
- [18] Selimefendigil, F., Öztop, H.F. (2014). Effect of a rotating cylinder in forced convection of ferrofluid over a backward facing step. *International Journal of Heat and Mass Transfer*, 71: 142-148. <https://doi.org/10.1016/j.ijheatmasstransfer.2013.12.042>
- [19] Anguraj, A., Palraj, J. (2018). Numerical study of fluid flow and heat transfer in a backward facing step with a rotating cylinder. *Malaya Journal of Matematik*, 6(2): 435-442. <https://doi.org/10.26637/MJM0602/0022>
- [20] Barsukov, A.V., Terekhov, V.V., Terekhov, V.I. (2021). Effect of a passive disturbance on the flow structure and heat transfer in the separation region behind a backward-facing step. *High Temperature*, 59(1): 115-120. <https://doi.org/10.1134/S0018151X21010028>
- [21] Abdollahpour, M., Gualtieri, P., Vetsch, D.F., Gualtieri, C. (2023). Numerical study of flow downstream a step with a cylinder part 2: Effect of a cylinder on the flow over the step. *Fluids*, 8(2): 60. <https://doi.org/10.3390/fluids8020060>
- [22] White, F.M., Majdalani, J. (2006). *Viscous Fluid Flow*. New York: McGraw-Hill.
- [23] Ahmed, M.A., Alabdaly, I.K., Hatem, S.M., Hussein, M.M. (2024). Numerical investigation on heat transfer enhancement in serpentine mini-channel heat sink. *International Journal of Heat & Technology*, 42(1): 183-190. <https://doi.org/10.18280/ijht.420119>
- [24] Versteeg, H.K. (2007). *An Introduction to Computational Fluid Dynamics the Finite Volume Method*, 2/E. Pearson Education India.
- [25] Pletcher, R.H., Tannehill, J.C., Anderson, D. (2012). *Computational Fluid Mechanics and Heat Transfer*. CRC Press.
- [26] Ferziger, J.H., Perić, M., Street, R.L. (2019). *Computational Methods for Fluid Dynamics*. Springer.
- [27] Ahmed, M.A., Alabdaly, I.K., Hatema, S.M., Hussein, M.M. (2023). Numerical investigation of hydrothermal performance and entropy generation through backward facing step channel with oval rib. *International Journal of Heat and Technology*, 41(5): 1349-1357. <https://doi.org/10.18280/ijht.410526>
- [28] Alabdaly, I.K., Ahmed, M.A. (2019). Numerical investigation on the heat transfer enhancement using a confined slot impinging jet with nanofluid. *Propulsion and Power Research*, 8(4): 351-361. <https://doi.org/10.1016/j.jprr.2019.06.004>
- [29] Ahmed, M.A., Hatem, S.M., Alabdaly, I.K. (2024). Investigation of heat transfer enhancement and entropy increment in a U channel with V-shaped ribs for improved hydrothermal performance. *International Journal of Heat and Technology*, 42(2): 455-465. <https://doi.org/10.18280/ijht.420211>
- [30] Mohsen, O.A., Muhammed, M.A., Hasan, B.O. (2021). Heat transfer enhancement in a double pipe heat exchanger using different fin geometries in turbulent flow. *Iranian Journal of Science and Technology, Transactions of Mechanical Engineering*, 45(2): 461-471. <https://doi.org/10.1007/s40997-020-00377-2>
- [31] Ahmed, M.A., Hatem, S.M., Alabdaly, I.K. (2023). Numerical examination of heat transfer and entropy generation in confined-slot jet impingement featuring wing ribs. *Power Engineering and Engineering Thermophysics*, 2(3): 173-187. <https://doi.org/10.56578/peet020305>
- [32] Ahmed, M.A., Alabdaly, I.K. (2019). Numerical study on hydrothermal performance factor using jet impingement and nanofluid. *Anbar Journal of Engineering Sciences*, 10(2): 308-315.
- [33] Armaly, B.F., Durst, F., Pereira, J.C.F., Schönung, B. (1983). Experimental and theoretical investigation of backward-facing step flow. *Journal of Fluid Mechanics*, 127: 473-496. <https://doi.org/10.1017/S0022112083002839>
- [34] Kim, J., Moin, P. (1985). Application of a fractional-step method to incompressible Navier-Stokes equations. *Journal of Computational Physics*, 59(2): 308-323.

NOMENCLATURE

<i>a</i>	Side length of square and diamond obstacles (mm)
<i>AR</i>	Aspect ratio (H/D)
<i>BFS</i>	Backward-facing step
<i>b</i>	Distance between step and obstacle (mm)
<i>C_p</i>	Specific heat (J/kg.K)
<i>D</i>	Circular obstacle diameter
<i>d</i>	Inlet channel height (mm)
<i>f</i>	Friction factor
<i>H</i>	Outlet channel height (mm)
<i>h</i>	Heat transfer coefficients (W/m ² .K)
<i>K</i>	Thermal conductivity (W/m.K)
<i>L</i>	Channel length (mm)
<i>Nu</i>	Nusselt number
<i>Pr</i>	Prandtl number
<i>PEC</i>	Performance Evaluation Criterion factor
<i>p</i>	Pressure (Pa)

<i>Q</i>	Heat flux (W/m ²)
<i>Re</i>	Reynolds number ($Re = \rho u_{in} D / \mu$)
<i>S</i>	Step height (mm)
<i>T</i>	Temperature (K)
<i>TBL</i>	Thermal boundary layer
<i>u, v</i>	Velocity components (m/s)
<i>x, y</i>	2D cartesian coordinates (mm)

Greek symbols

Δp	Pressure drop (pa)
ρ	Density (kg/m ³)
μ	Dynamic viscosity (N.s/m ²)

Subscripts

<i>ave.</i>	Average
<i>in</i>	Inlet
<i>out</i>	Outlet